ON THE SUB-CLOUD LAYER STRUCTURE RELATIVE TO CUMULONIMBUS SYSTEMS IN VENEZUELA

by

PEDRO P. PACHECO

DEPARTMENT OF ATMOSPHERIC SCIENCE
COLORADO STATE UNIVERSITY
FORT COLLINS, COLORADO

ON THE SUBCLOUD LAYER STRUCTURE RELATIVE TO CUMULONIMBUS SYSTEMS IN VENEZUELA

by

Pedro P. Pacheco

ABSTRACT

ON THE SUBCLOUD LAYER STRUCTURE RELATIVE TO
CUMULONIMBUS SYSTEMS IN VENEZUELA

In this report properties of the subcloud layer are examined with respect to cumulonimbus systems as seen by radar over eastern Venezuela during project VIMHEX I of 1969. Two meso-networks were maintained during this project within the radar circle of 100-km radius. One of these consisted of surface stations measuring temperature and humidity. The second was a net of nephoscope stations designed to measure wind vectors at low cloud base and from these establish the meso-circulations with respect to cumulonimbi. It is believed that this is the first time in meteorological history that such a network has been employed.

The wind data show that the cumulonimbi move faster than the low-level wind. Since the winds are largely from the east, the relative wind is from the west, and air enters the clouds at their leading edge. Mass convergence around the echo center is found to be small, presumably due to the fact that many of the measured winds are indicative of the period before onset of heavy convection. The vorticity analysis reveals a change from cyclonic relative vorticity on the outskirts to anticyclonic vorticity on the echo edge. Conversion of horizontal to vertical vorticity must account for this field. Observed horizontal vorticity fields are examined. Normally the easterly shear is positive below 700-600 mb. Assuming that this is the layer of main importance in the present context, a vertical circulation about the easterly current is obtained that will explain the vorticity fields and also the tendency of the echo tracks to deviate to the right of the middle tropospheric winds.

Analysis of surface energy shows that both sensible and latent heat are reduced during convection, hence also total energy. Such a decrease can only happen through importation of lower energy air from upper levels, verifying previous analyses which suggested that the down-drafts actually effect a vertical exchange of mass. Further, during the incipient echo stage, concentration of high moisture and temperature is found upstream along the relative motions paths from the echoes. It is suggested that mesoscale area of high and low energy of the surface air actually exist prior to onset of convection and that the cumuli which grow to cumulonimbus are located where surface energy content is highest.

ACKNOWLEDGEMENT

This research was performed while the author was on scholarship from the Meteorological Service of the Venezuela Air Force to Colorado State University. Project VIMHEX I, directed by Professor Herbert Riehl, was a joint enterprise of Colorado State University, under a research grant from the Office of Naval Research, and agencies of the Venezuelan Government. The author wishes to thank Professor Riehl for his patient supervision and encouragement during the time it has taken to complete this work. Special thanks are also due to Miss Karla Garretson and Mrs. Pat Johnson for computation and typing assistance, as well as many others who have made contributions to this effort.

INTRODUCTION

During June to September 1969 Project VIMHEX I (International Meteorological and Hydrological Experiment, Phase I) was carried out in northeastern Venezuela with headquarters at Anaco (Fig. 1). One objective of this experiment was to establish time histories of individual cumulonimbus cloud systems and using these, to make a contribution to knowledge on interaction between cumulonimbus and synoptic disturbances and the general circulation.

The principal research instrumentation at Anaco consisted of a modified M-33 radar and a rawinsonde installation from which balloons were sent up as frequently as possible during periods with convective activity. From the radar photos Cruz (1972) extracted the histories of the radar echoes outlining the cumulonimbi while Betts (1972) computed the exchange of mass and energy between the cumulonimbus systems and their environment. According to the initial plan for the experiment, the rawinsonde observations were placed in a coordinate system centered on a particular radar echo. Analysis then was performed of all balloon-derived observations thus accumulated.

It was realized early that the rawinsonde observations give rather little information on the subcloud layer and that, with radar echoes often up to 80 km distant from the radar-rawinsonde site, it would be desirable to gather additional observations especially helpful for subcloud layer analysis. For this purpose a net of surface stations was established with measurements of temperature, humidity, rainfall and wind (Fig. 2). Further, another net of nephoscope stations was developed, also seen in Fig. 2. The purpose of this network was to make

observations of the motion vector of the low clouds at their base. Assuming that there is little turning of wind with height in the lowest kilometer, the layer mainly below cloud base, the data from the meso-network of nephoscopes would be suitable to establish the mesostructure of air motion, divergence and vorticity relative to radar echoes in different phases of their life cycle. It is believed that such a meso-network, while often talked about, was never put into operation prior to VIMHEX I. If, in addition, the subcloud layer could be assumed to be reasonably well mixed, the combination of nephoscope winds and surface temperatures and humidities should yield the transport of sensible heat and moisture in and out of cumulonimbi below cloud base. Such a computation would be a valuable adjunct to the rawinsonde analyses of Betts (1972).

The objective of this study, thus, was to place the observations from both meso-networks in a coordinate system relative to radar echoes during ascending and descending phases of large echoes as defined by Cruz (1972), and then to perform the calculations indicated above.

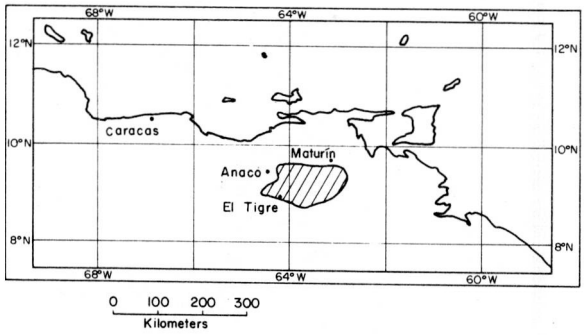

Figure 1. Location of experimental area in 1969. Anaco was headquarters. Shading indicates watersheds for hydrologic computations.

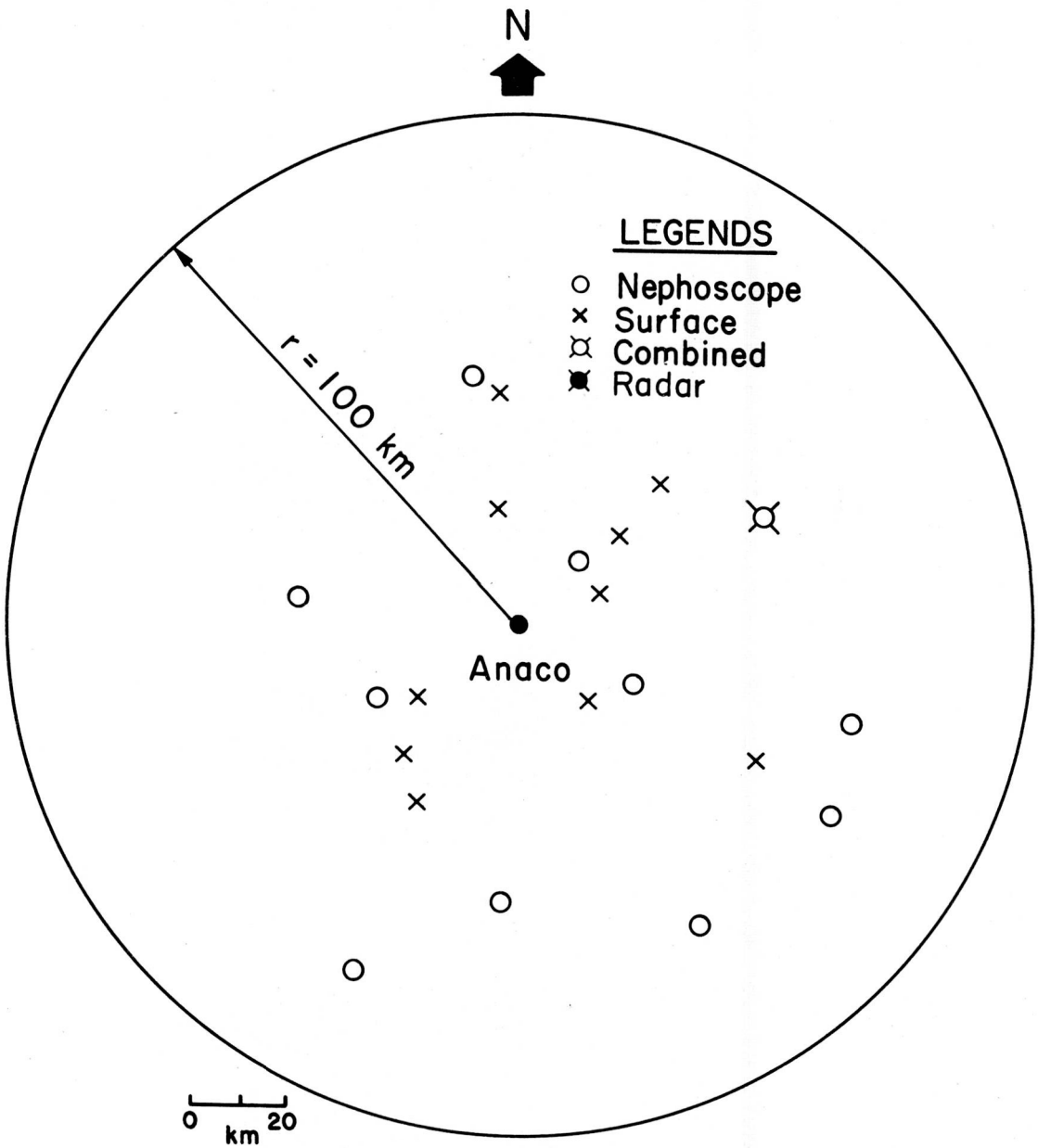

Figure 2. Location of meso-networks within radar circle.

METHODS OF ANALYSIS

Basic Data: The network of surface stations was operative mainly during August - September 1969. Strip recordings of temperature and humidity were collected weekly from the stations and later put on punchcards in form of hourly observations at the Climate Center of the Weather Service of the Venezuelan Air Forces. These hourly values furnished part of the data input. Observations collected from the nephoscope stations had to be evaluated making some assumption about the cloud base height. The assumption used was that the cloud base was located at the convective condensation level determined from surface temperature and dewpoint during daytime. This assumption, generally regarded as a good approximation, was verified at Anaco with a ceilometer during several periods with extensive low cumulus cover which permitted the ceilometer to function. However, it must be mentioned that, while the rawinsonde data gave an adiabatic temperature lapse rate below cloud base, they did not show uniform moisture. The decrease of specific humidity with height in the subcloud layer was enhanced artificially by response of the radiosonde instrument to sunlight, as noted by various investigators concerned with the U. S. radiosonde used in 1969. Nevertheless, after corrections applied by Betts (1972), there still remained a residual moisture gradient of 3-4 g/kg in the subcloud layer, mostly concentrated between the surface readings and 950 mb, a layer 1,000-ft thick, as seen from the mean soundings of Riehl, et al. (1972). Betts and others have preferred to use a mean specific humidity of the subcloud layer rather than rely on the surface temperature-dewpoint spread to determine cloud base height and energy at cloud base. There is here a residual element of uncertainty

in the validity of the nephoscope observations which is expected to be dealt with only during the second stage of VIMHEX in the summer of 1972 when systematic double theodolite measurements of cloud base are scheduled and to be correlated with temperature-dewpoint spread.

With the assumption about cloud base height discussed, the wind vector at cloud base was readily generalted by a small machine computation program. Original observations were made hourly, so that hourly values were available for subsequent analyses. It turned out that low cloud bases generally existed on convective days only during the morning and noon hours. With the development of cumulonimbus in the afternoon, low trade wind cumuli usually disappeared and were replaced by altostratus, often based at 3 km or higher, indicative of drying of the lower atmosphere through downdrafts from cumuli. Such downdrafts have been noted in recent literature (Riehl, 1965) over the ocean. Even there the cloud base has been observed to rise dramatically to 3 km; but on account of the ever available energy supply at the ocean surface high dewpoints and cumuli with low bases may reappear quickly, whereas over land low cumulus bases usually have not been observed to recur until the following morning. Thus, useful nephoscope observations were restricted mainly to the period with onset of the first cumulonimbus systems. When it is further considered that the networks mainly operated during August - September 1969, that September was a dry month yielding little data and that all operations were intermittent only, it can be seen that the observational sample of radar echoes to be studied was very small. In fact, compared to 232 echoes analyzed by Cruz (1972) and 15 cases possessed sufficiently complete data to be considered here, a sample more than an order of magnitude smaller.

Wind Analysis: The 15 cases were divided into a growing and a decaying stage each according to the histograms of echo height and area. In order to combine all echoes, a non-dimensional radius had to be introduced for normalization of echo size (cf. also Betts, 1972). This radius is defined by $\frac{x'}{r'} = \frac{r}{r_o}$, where r_o is the averaged echo radius. Hence $r' = 1$ by definition at the echo edge. During the growing stage the actual echo radius averaged 8 km, during the decaying stage 12 km, so that echo area doubled.

The question of echo direction of displacement was considered. In the analysis by Betts (1972) all wind fields rotated so that all directions of cloud motion became coincident. After some early tests this technique was abandoned for present purposes. Direction of the low level winds varied little, and some rather unrealistic patterns developed when the rotation was carried out. Hence, in the end, the actual wind directions were used. Individual wind vectors were placed relative to the echo center with the non-dimensional radius as coordinate and then averaged vectorially in small squares with length of side corresponding to $\Delta r' = 2$, yielding 36 point values. The resulting streamline fields were easterly to southeasterly. Only at this point was the averaged displacement vector of the echoes introduced and subtracted. The resulting composite relative motion field, derived by the method just described, forms the basis for the later discussion.

Analysis of Temperature and Specific Humidity: Two problems had to be dealt with in averaging hourly values of temperature and specific humidity in relative coordinates. One of these is described by Riehl (1972): In and after showers at a station, the total energy as measured in thermometer shelters often goes up, whereas at most it should remain

constant and more probably decrease in case of downdrafts. It is suggested that this effect is due to storage of solar energy in the wood of the shelter itself and not a real feature of the atmosphere. Hence 11 observations during and after precipitation had to be screened for unrealistic energy values and the observation omitted in such instances.

Second, whereas specific humidity has little diurnal variation and could be included without correction within the limits of accuracy of all calculations, the same cannot be said for dry-bulb temperature. The latter, as is normal, undergoes a distinct rise in the morning and noon hours, generally on the order of 10C, and this diurnal rise had to be normalized if temperature observations from different hours were to be averaged. The following technique was devised: At first a diurnal temperature curve was established from the data for all stations for days with active convection as considered in this study; this should be better than using general climatic temperatures at different hours. Then the difference between individual temperatures and the average temperature at each hour was determined; this temperature deviation, T', was plotted and averaged in small areas just as for wind yielding 36 points for analysis.

STRUCTURE OF THE WINDFIELD

Figures 3 and 4 show relative streamlines and isotachs for ascending and descending echo phases. The general change of the relative direction from west to northwest between Figs. 3 and 4 comes mainly from a northwestward turning of the echoes rather than from a change of cloud base wind direction. It is the major result of the wind analysis that the echoes propagate more rapidly than the trades, i.e., the relative wind is from west to northwest whereas the actual wind is east to southeast. The same feature is encountered in the low-level rawinsonde plots (Betts, 1972) whereas in the middle troposphere echo speed and wind speed appear fairly well correlated (Cruz, 1972). While the present data are not suitable for further analysis of this remarkable fact, it may be suggested that such relative motion is plausible given a tropospheric wind structure with clockwise vorticity about the horizontal axis pointing perpendicular to the right of the echo propagation. Then, if the growing towers are located upshear as suggested by construction of the horizontal vorticity components, verified by many time-lapse cloud models, the dynamic component of echo displacement would be additive to the translatory component resulting in relative motion from the west in the trades. It may be mentioned that further observations concerning this hypothesis are planned for VIMHEX II.

While, in both phases, the low-level air is accelerated along the relative streamlines pointing toward the echo area, wind speed distribution in general is rather erratic, leading to irregular patterns of divergence. The echo area (Fig. 5 a-b) has convergence in both phases, strongest during growth of echo; divergence prevails to the west.

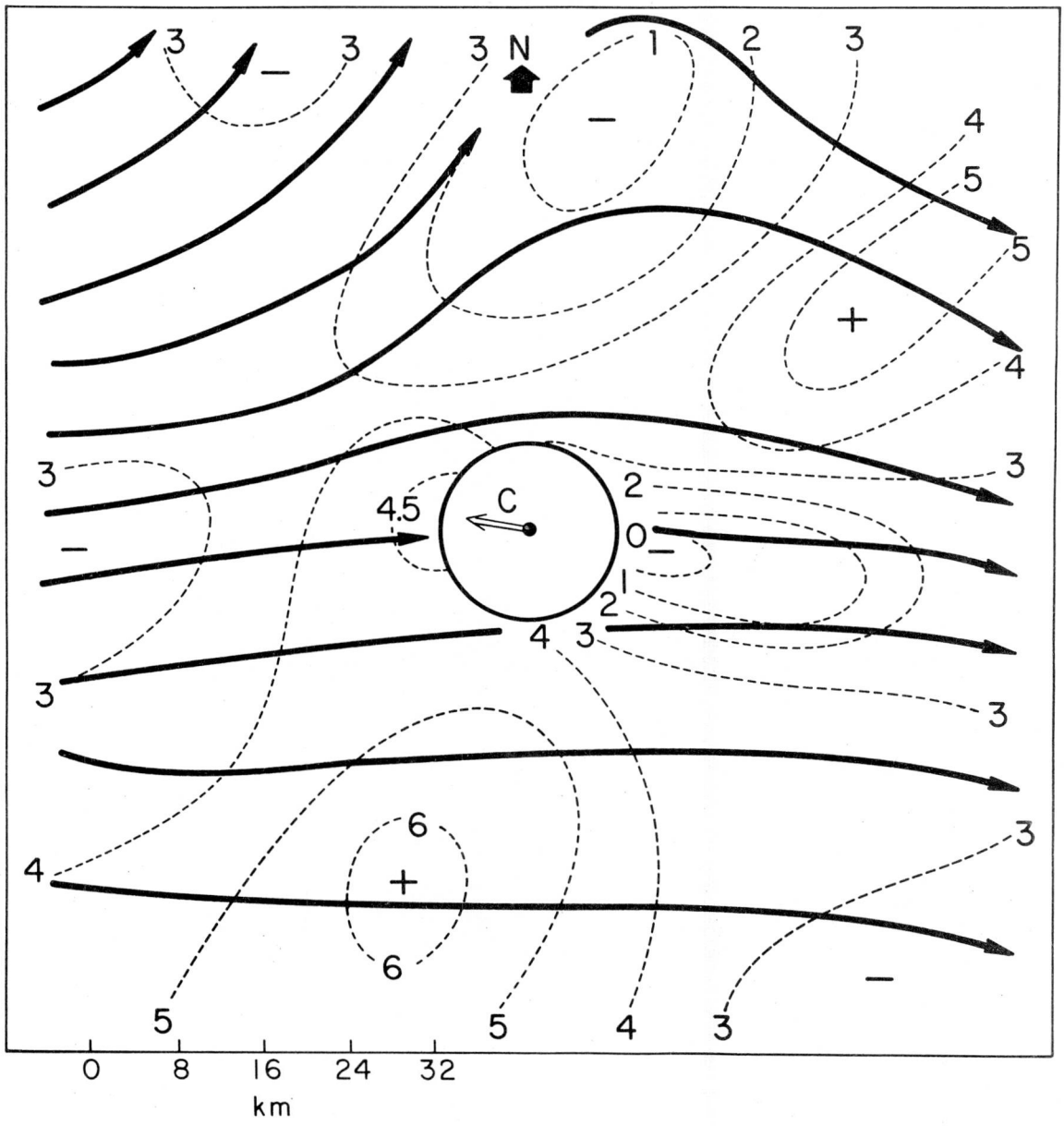

Figure 3. Streamlines and isotachs (m/s) of the wind at cloud base to echo motion. Direction of echo motion (C) shown within radar echo circle. For ascending phase of echoes. Distance scale for average echo size given at bottom.

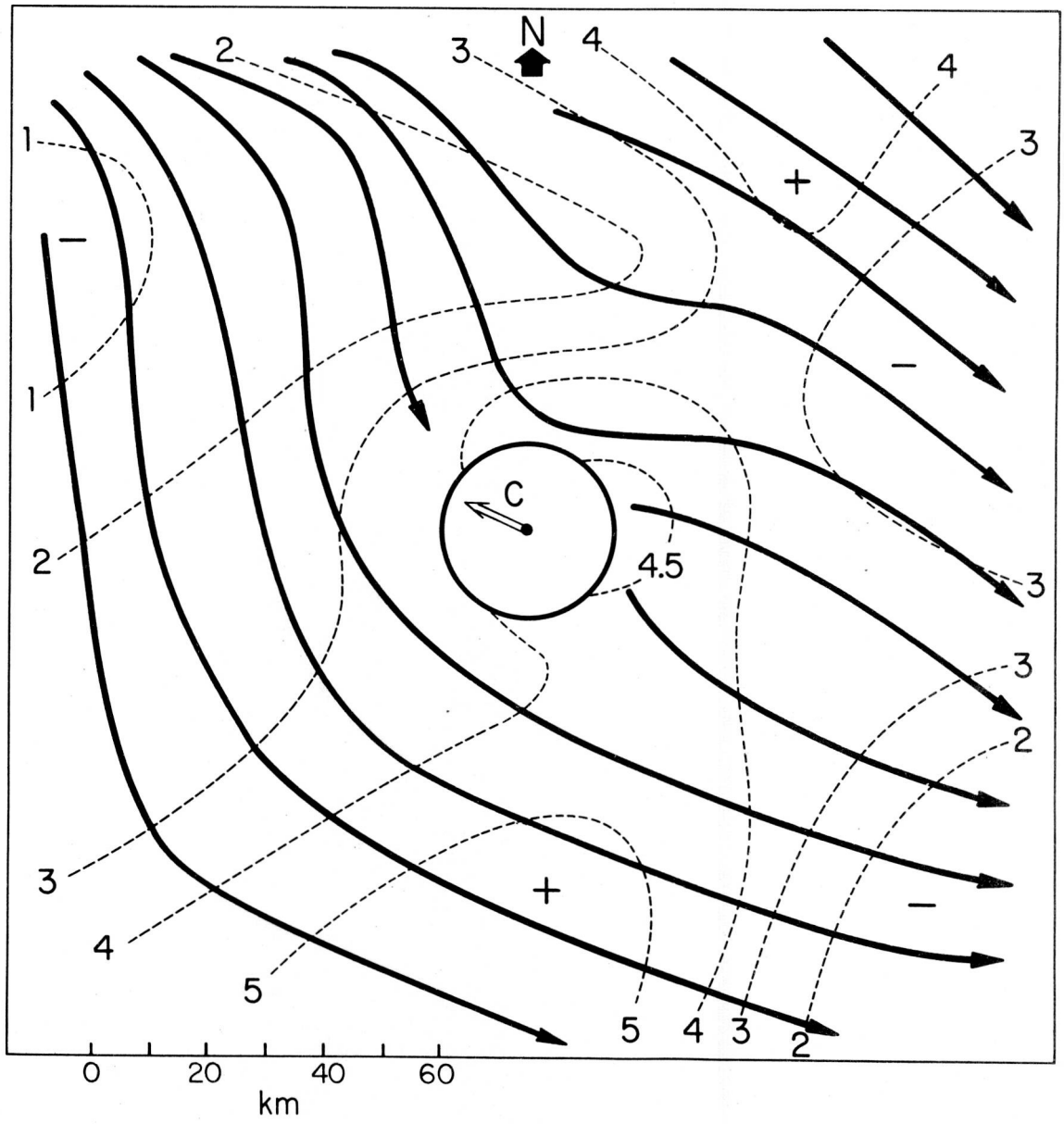

Figure 4. Streamlines and isotachs (m/s) of the wind at cloud base to echo motion. Direction of echo motion (C) shown within radar echo circle. For descending phase of echoes. Distance scale for average echo size given at bottom.

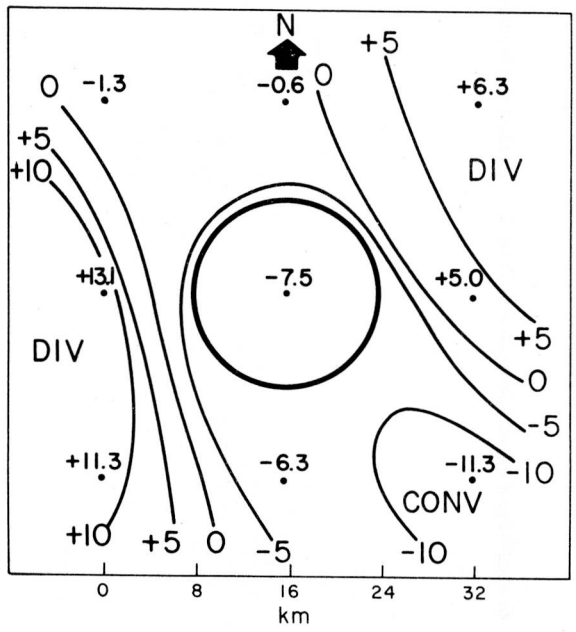

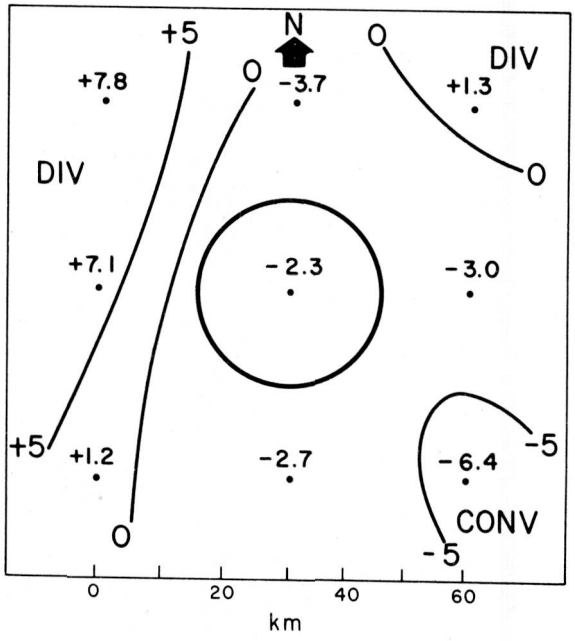

Figure 5. (a) Divergence (10^{-5} sec^{-1}) for ascending phase. Distance scale for average echo size given at bottom; (b) divergence for descending phase.

However, a marked convergence area also appears in the southeast which is not readily explained. Further, the divergence values are small yielding vertical motions with only a magnitude of 10 cm/sec within the echo area in Fig. 5a, assuming the divergence field holds for the entire subcloud layer of 100-mb pressure thickness. Of course, larger vertical motions of 1 m/sec magnitude would be obtained if it is postulated that the ascent is concentrated in towers rising at the western echo edge in correspondence with the horizontal vorticity model. More detailed calculations are not possible. It may be added that numerous winds entering into Fig. 5a stem from a time before echo start, hence are indicative only of general onset of a convergent field rather than of cumulus-scale convergence itself.

The analysis of relative vorticity about the vertical axis yielded an unexpected result (Fig. 6 a-b). Magnitude is somewhat larger than that of the Coriolis parameter (2.3×10^{-5} sec^{-1}); however there is no order-of-magnitude difference. We find cyclonic vorticity in the outskirts of the area analyzed during both phases, and anticyclonic vorticity around the echo area. Possibly, the accuracy of the nephoscope observations is too marginal to establish the vorticity distribution with certainty. However, even if only the gross features are correct, such a distribution can only be brought about by transformation of horizontal into vertical vorticity. The relevant terms in the vertical vorticity equation are

$$\frac{d\zeta}{dt} = \eta \frac{\partial w}{\partial n} \qquad (1)$$

where ζ is vertical relative vorticity, η horizontal vorticity as defined earlier, w vertical velocity and n horizontal distance along

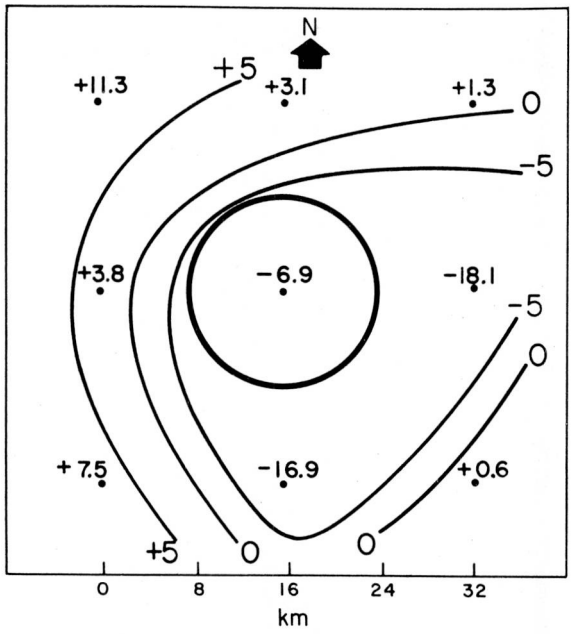

(a)

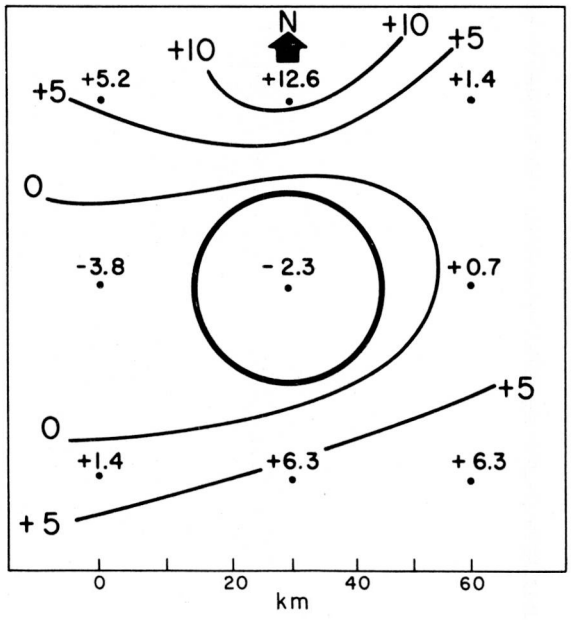

(b)

Figure 6. (a) Vertical component of relative vorticity (10^{-5} sec^{-1}) during ascending phase of echoes; positive values denote rotation in Northern Hemisphere sense. Distance scale at bottom for average echo size given at bottom; (b) vorticity for descending phase.

η . We shall assume, for computational purposes, that $\frac{d\zeta}{dt} = V_r \frac{\partial \zeta}{\partial s_r}$, where V_r is the relative motion along the relative streamline s_r . Further, we take $\eta = \partial u/\partial z$, where u is the wind component along the direction of echo propagation and z the vertical coordinate. We shall try

$$\eta = + 10 \text{ mps}/10 \text{ km} = 10^{-3} \text{ sec}^{-1} ,$$

i.e., a weak shear from trades to high-tropospheric westerlies. Further, from Figs. 3 and 6

$$V_r \frac{\partial \zeta}{\partial s_r} = 5 \text{ mps} \times (-10 \times 10^{-5} \text{ sec}^{-1})/20 \text{ km} = -2.5 \times 10^{-8} \text{ sec}^{-2} .$$

Here, the scale at the bottom of the illustrations using the mean echo radius for distance has been adopted. If the distance n across the echo is also taken as 20 km, it follows that $\Delta w = -50$ cm/sec, revolving clockwise as seen by an observer looking down the actual low-level streamlines; i.e., in the trades the clouds would build on the southside and dissipate on the northside. This result does not agree with the findings of Cruz (1972) who noted that echoes tended to deviate to the right rather than to the left of the mid-tropospheric wind in the majority of his cases. It may be more relevant to define $\partial u/\partial z$ for the layer surface-700 mb rather than for the whole troposphere when equation (1) is applied to the subcloud layer and to the lower parts of the cloud layer. In this portion of the troposphere $\partial u/\partial z$ is usually positive easterly with magnitude still of 10^{-3} sec^{-1}. Thus, if this interpretation is valid, the inverse picture of the one presented above would be correct, i.e., the rotation would be counterclockwise for an observer looking down the streamlines, and the echoes would deviate to the right of the mid-tropospheric wind. A consistent

picture of echo displacement and meso-scale vertical vorticity would thereby be obtained; however, the counterclockwise rolls have not yet been proved to exist, nor is a reason for such consistent rotation evident.

TEMPERATURE AND HUMIDITY ANALYSIS

Total Energy Variation: The main objective in establishing the network of surface stations during VIMHEX I was determination of the changes in surface energy accompanying cumulonimbus systems, especially by means of the downdrafts associated with them. As has been well established for many years, cooling accompanies rain showers. But in general such cooling has been ascribed to evaporation of falling rain, a process which takes place at constant energy. Recent investigations (Riehl, 1965, Zipser, 1969) have found, in contrast, that both temperature and moisture decrease in the surface layer over sea, hence a reduction of total energy occurs. Such reduction can only happen if downdrafts from the lower and middle troposphere actually import low-energy there situated toward the surface leading to a general mixing of the low troposphere. The effect on total energy is the same as experienced during cold front passage, except that in this case the low-energy air does not arrive from higher latitudes but from higher altitudes. A downdraft effect can be seen very clearly on radiosonde records made near or after the end of the convective period when compared to soundings before and during convection. As illustrated in Fig. 7, sharply lower humidity is carried as far down as the 950-mb level resulting in a large temperature-dewpoint spread in the subcloud layer.

At the surface, all temperatures and specific humidities were averaged for the increasing and decreasing echo phases, indicating a temperature decrease (measured in terms of deviations with respect to hourly averages as discussed earlier) of 5C and a decrease in specific

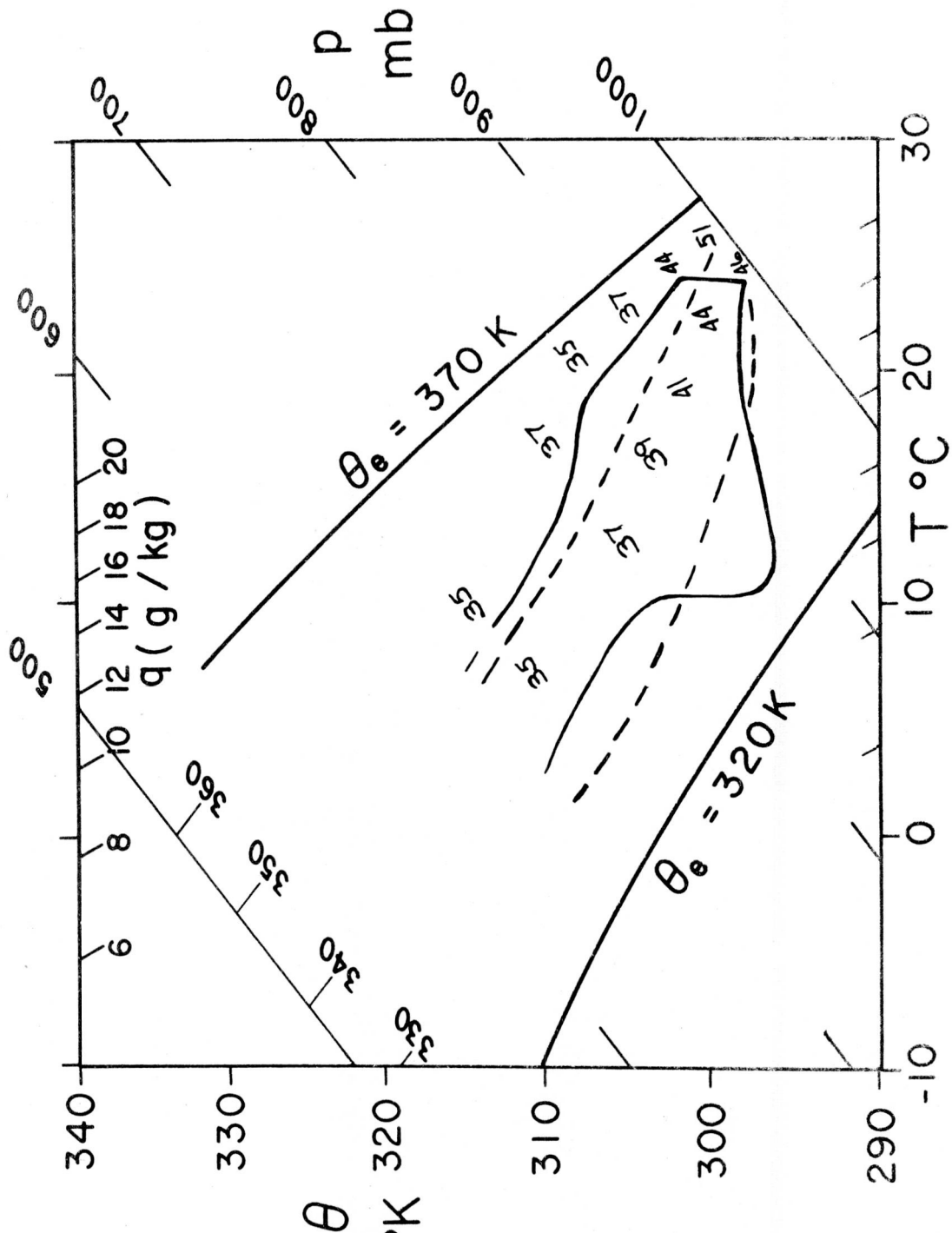

Figure 7. Tephigram showing composite temperature and dewpoint sounding typical for the stage after termination of convection (solid) and composite sounding during convection activity (dashed). Note especially the intrusion of drier air into the atmosphere.

humidity of 2.5 g/kg. As already stated, certain observations showing an increase in total energy were omitted from the calculations, and this may be thought as biasing the sample. However, only a fraction of observations in the immediate rain area of cumulonimbi were eliminated. The data here presented indicate the bulk effect of downdrafts spread over the entire area with a sample of about 150 observations.

The change in total energy (Q) is given by

$$\Delta Q = c_p \Delta T + L \Delta q \quad , \tag{2}$$

where c_p is specific heat at constant pressure, T temperature, q specific humidity and L latent heat of condensation. The term $c_p T$ gives the specific enthalpy and Lq the latent heat energy. Potential energy does not appear since the variations occur at constant altitude, and kinetic energy is omitted as a negligible quantity in the present context. From equation (2) we obtain that Q = -2.8 cal/gm from the early to the terminal stage of cumulonimbus convection. In terms of equivalent potential temperature, we consider the relation

$$\Delta \theta_e = 1.17 \ (\Delta T + 2.5 \ \Delta q) \tag{3}$$

and find that $\Delta \theta_e$ = - 14K. Initially, with average potential temperature of 304K and specific humidity near 20 g/kg, θ_e = 360K. Thus, after convection, θ_e = 346K. As may be seen from the wet sounding composite of Riehl, et al (1972) this decrease indicates no more than fairly thorough mixing down of subcloud layer air and may be compared with the equivalent potential temperature gradient of the soundings in Fig. 7. Evidently,

verification for the downdraft mechanism importing lower energy air toward the surface has been obtained.

Temperature and Humidity Fields: Only the ascending stage will be treated here, since it proved impossible to analyze fields of the descending stage. Distribution of temperatures and specific humidities was quite irregular in that stage; conclusions could be drawn only concerning the average energy values over the whole area as just presented.

During the ascending stage a considerable amount of variability also was encountered, as is reasonable in a field in which average gradients really are not expected to occur. There is no a priori reason to assume that meso-scale temperature and moisture analysis would yield any distinct pattern. Yet a pattern was found. In Fig. 8 we see the moisture deviation from the average for the early stage. The labeling "greater than" on the $q' = 1.5$ g/kg line indicates that the majority of data points in the area enclosed by this line had deviations greater than +1.5 g/kg. However, because of the variability mentioned, lower positive and even a few negative values are also present. The zero isoline must be understood in the same sense. And beyond the zero line deviations are predominantly negative, yet with a few interspersed positive values.

Figure 8 suggests that streaks with higher and lower moisture must occur on the meso-scale in the area and that incipient cumulus clouds line up so that the relative wind carries the high moisture concentration. The whole experimental area is very flat and uniform in underlying surface; it was especially picked for that reason, so that preferred point of convection origin or path of echoes would be minimized. It is suggested that Figs. 8-10 may be examined without having to take local topographic

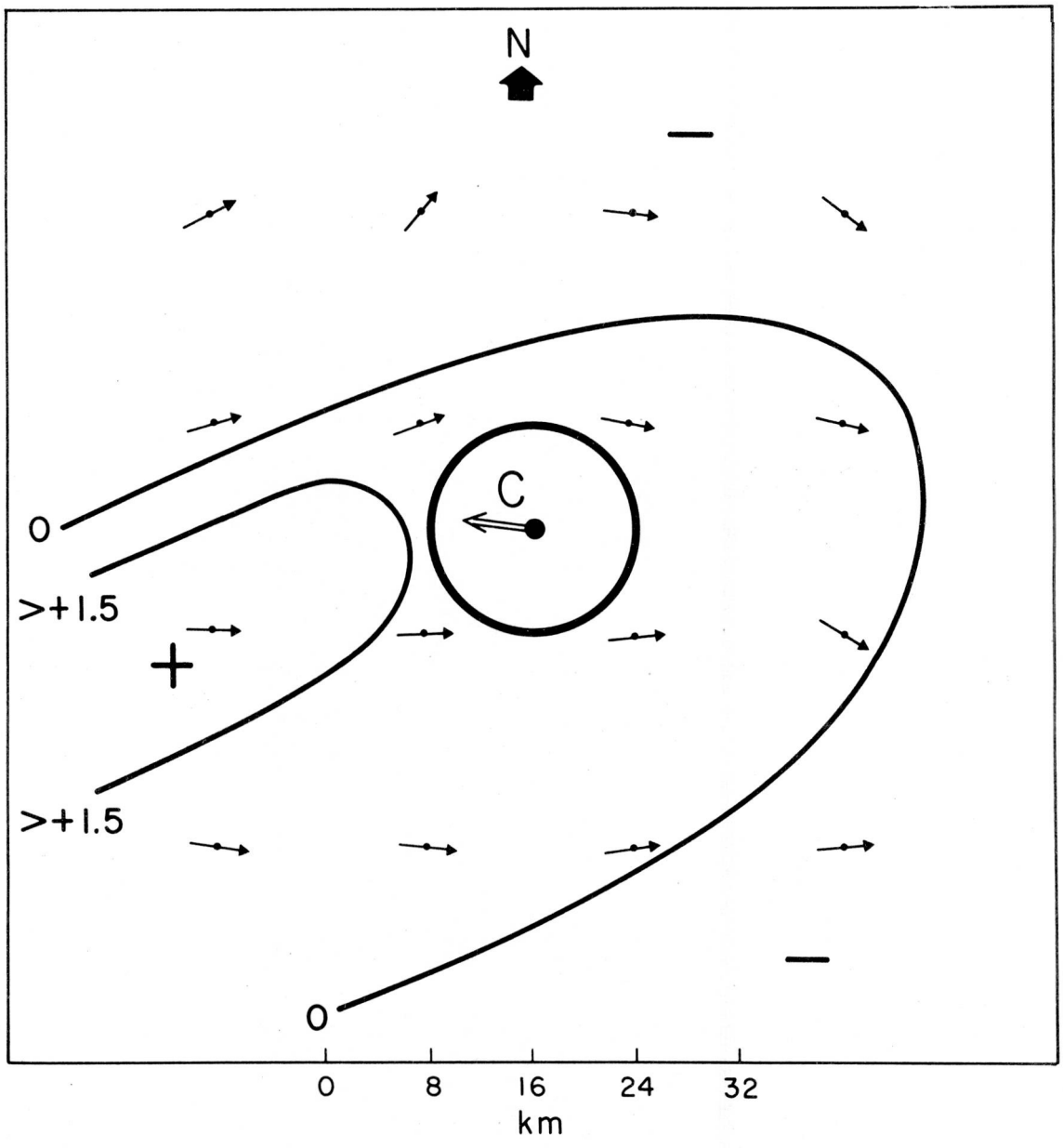

Figure 8. Deviation of specific humidity from average for the chart (g/kg) and relative motion vectors for ascending phase from Figure 3.

factors into account. If so, the existence of meso-scale moisture fields near the time of onset of convection is demonstrated, irrespective of any explanation for these fields which may, in part, be leftovers from the downdrafts of the previous day's convection.

The surface temperature field (Fig. 9) can be analyzed in the same way as the moisture field. High sensible heat, associated with high moisture, is imported toward the initial echo area with the relative winds from west. However, cooling occurs before the echo edge is reached; the whole radar circle is relatively cold even at the onset of convection. It is difficult to assign a mechanism to the cooling. One plausible suggestion is that, with increasing surface wind speed and with velocity divergence as shown earlier, mechanical turbulence is enhanced and superadiabatic temperature lapse rates near the ground reduced. Alternately, we may suppose that cumulus cloud formation begins well upstream from where these clouds become visible on the radar screen. In that event, shading from sunlight could affect surface temperature, especially since travel time from the edge of the area with decreasing temperature to the echo edge is at least half an hour from Fig. 3. No proof can be furnished for either of these hypotheses. The main result of Figs. 8 and 9 is that meso-scale patterns of heat and humidity do appear to exist near the onset of convection, and that the growing cumuli with preference occur along the relative trajectories of high energy of the surface layer.

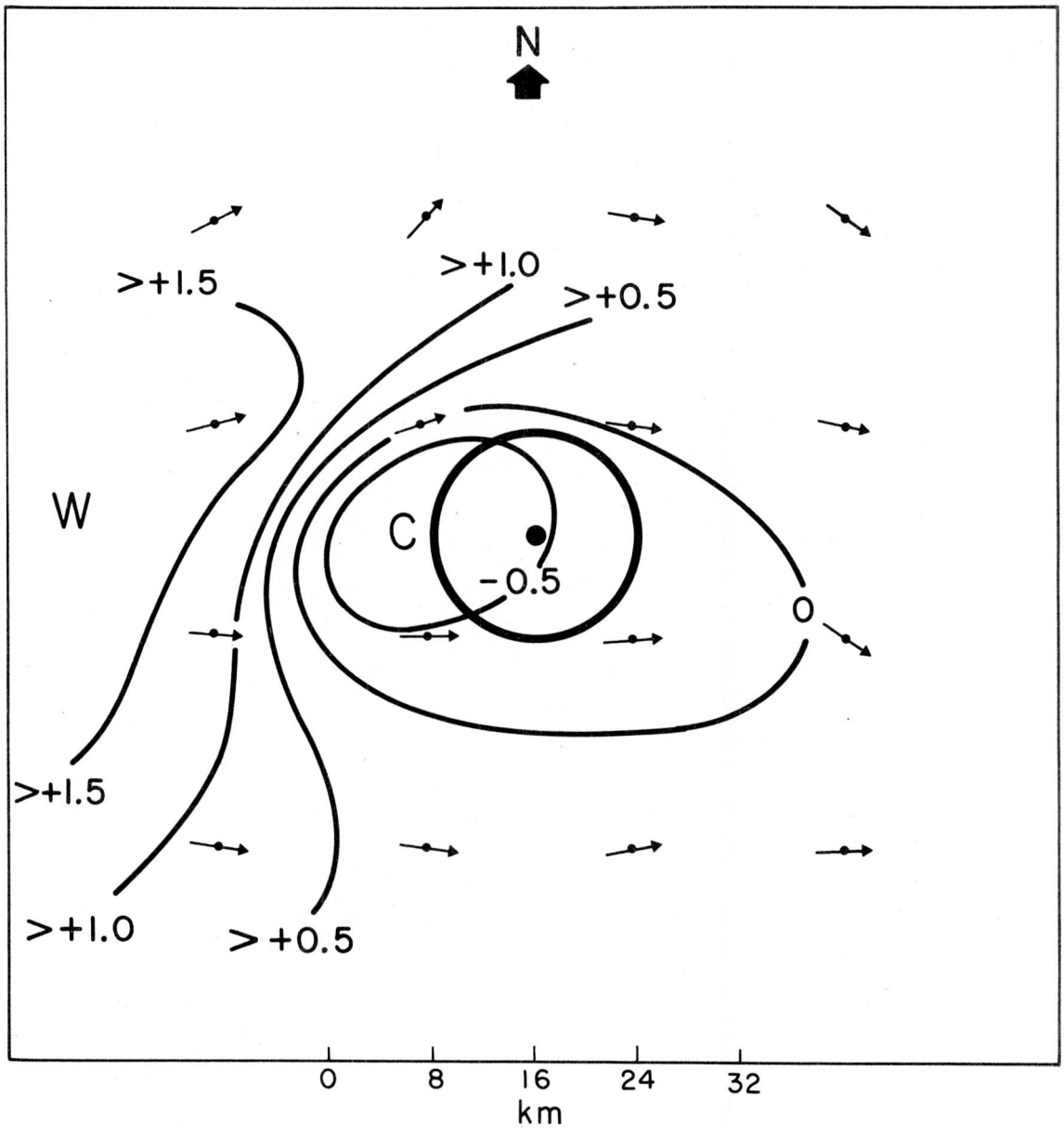

Figure 9. Temperature deviation analysis as defined in text (^{o}C) and relative motion vectors for ascending phase.

REFERENCES

Betts, A. K., 1972: A composite mesoscale cumulonimbus budget. Paper presented at the annual meeting of the AGU in Washington, D. C., April 17-21.

Cruz, L. A., 1972: Venezuelan rainstorms as seen by radar. Paper presented at the annual meeting of the AGU in Washington, D. C., April 17-21.

Riehl, H., 1965: Varying structures of waves in the Easterlies; Chapter X, Dynamics of Atmospheric Processes in Tropics; Dynamics of Large-Scale Atmospheric Processes. Proceedings International Symposium, Moscow, June 23-30, 411-416. Atmospheric Science Technical Paper #117, Colorado State University.

_____, L. Cruz, M. Mata, and C. Muster, 1972: Precipitation characteristics during the Venezuelan rainy season. Paper presented at the annual meeting of the AGU in Washington, D. C., April 17-21.

Zipser, E. J., 1969: The role of organized unsaturated convective downdrafts in the structure and rapid decay of an equatorial disturbance. Journal of Applied Meteorology, Vol. 8, No. 5, October, 799-814.